Adaptive Finite Element Methods for Low Mach, Steady, Laminar Combustion

Erik Burman

DMA, Ecole Polytechnique Fédérale de Lausanne, CH-1015, Switzerland

and

Alexandre Ern

CERMICS, Ecole Nationale des Ponts et Chaussées, 6 et 8 avenue Blaise Pascal, F-77455 Marne la Vallée cedex 2, France

and

Vincent Giovangigli

CMAP, Ecole Polytechnique, F-91128 Palaiseau cedex, France

We investigate adaptive finite element methods for low Mach, steady, laminar combustion. The finite element discretization of the flame equations involves least squares control of streamline derivatives and pressure-velocity coupling as well as a new shock capturing term based on nonlinear crosswind diffusion yielding a suitable discrete maximum principle for the discrete solution. A posteriori error estimates derived from a dual weighted residual method are used to refine the mesh adaptively. Numerical results are presented for a Bunsen flame with simple chemistry on locally refined as well as fully unstructured Delaunay meshes. Solution quality is evaluated in terms of overall flame characteristics—including length, lift off and width—and undershoots in species and temperature profiles.

Key Words: combustion, finite elements, adaptive mesh refinement, Bunsen flames, a posteriori error estimation, shock capturing

1. INTRODUCTION

The numerical computation of reactive flows is a challenging field of research with many applications in science and engineering. Most combustion applications involve strongly nonlinear phenomena, such as reaction fronts, boundary layers, turbulence or shocks. The computational work involved in flame simulations is extremely high

because of the wide spectrum of spatial and time scales to be resolved, the large number of degrees of freedom and strong nonlinearities resulting from chemical reactions.

The goal of this paper is to derive suitable numerical methods for flame simulation. Targeted combustion applications are low Mach, steady, laminar flames such as those encountered in Bunsen flames and other commercial burners. Key issue in a numerical method is *reliability*: once an approximate solution has been obtained, there should be a computable estimate of the numerical error indicating whether or not the computed solution meets the user's accuracy requirements. An additional important feature of a numerical method is *efficiency*, i.e., to achieve reliability at low computational costs.

An attractive approach to achieve efficiency in flame simulations is to resort to adaptive methods where the computational mesh adjusts itself to fit the nature of the numerical solution. A first strategy for adaptive mesh refinement relies on one-dimensional mesh equidistribution using local estimates of the gradient and curvature of the numerical solution as error indicators [KN80, Che94]. This methodology has been applied to steady [GS89, CP93, dd94, Mdvd95, Sd95] and unsteady [PHB+98, Pax99, DB00] flame simulations. Recent developments include local rectangular refinement techniques with finite difference discretizations [BS99, BS98]. In most applications involving several nonlinear partial differential equations (PDEs), the error indicators lack theoretical justification and therefore strongly rely on problem oriented heuristics. Another drawback is that no reliable criterion for stopping the simulation is available due to the lack of computable estimates of the actual numerical error.

One alternative approach toward adaptive error control has been developed recently in the framework of finite element methods and optimal control techniques [BR96, BR01]. Let u be the exact unknown solution and u_h a numerical approximation. Given a functional $J(\cdot)$ representing the physical quantities that the user wishes to control, an upper bound for $J(u) - J(u_h)$ is obtained using the dual weighted residual method. The estimate involves the residual, defined as the numerical solution reinjected into the differential equation, and appropriate weight factors. Such factors, which can also be interpreted as sensitivity coefficients, are computed from the solution of a linearized dual problem and provide information on where the error is actually generated. The dual weighted residual method exploits the Galerkin orthogonality in deriving the local weights. This property is satisfied by finite element approximations but usually not by standard finite difference or finite volume discretizations. The dual weighted residual method offers the important advantage to address both reliability and efficiency. Indeed, it provides a reliable criterion for stopping the simulation and it also yields practical information for adaptive mesh refinement. The error estimator is localized as a sum over all the mesh elements and a refinement/derefinement algorithm can be readily set up for instance by equidistributing the element contributions. This method has been applied to combustion problems in [Bra98, BBR99]. Linear quadrangular finite elements with streamline and velocity-pressure stabilization were used on adaptively refined meshes with local tensor product structure and hanging nodes.

In this paper, we present an adaptive finite element method to simulate low Mach, steady, laminar flames. The flame equations are discretized with linear sim-

plicial conforming elements on either locally refined or fully unstructured Delaunay meshes. The stabilization involves streamline diffusion, pressure-velocity coupling as well as a new shock capturing term. This term is based on a nonlinear crosswind diffusion operator ensuring a suitable form of the discrete maximum principle for temperature and species profiles [BE01]. Although this work is restricted to steady flames, the finite element method presented hereafter is readily extendable to unsteady problems. The paper is organized as follows. In section 2 we present the governing equations. The stabilized finite element discretization is presented in section 3. Section 4 describes the dual weighted residual method for adaptive mesh generation. Both theoretical aspects and practical implementation are highlighted. Finally, computational results are presented in section 5. We investigate solution quality in terms of undershoots for temperature and species profiles, flame length, lift off and width. Various shock capturing techniques based on crosswind diffusion are compared.

2. GOVERNING EQUATIONS

The governing equations of chemically reacting flows express conservation of species mass, momentum and energy. We focus on low Mach, steady, laminar flames such as those arising in Bunsen and other commercial burners (see figure 1). A premixed fuel/oxidizer jet is flown through a cylindrical tube surrounded by an air coflow. When the jet velocity exceeds the planar flame speed, it is possible under certain experimental conditions to stabilize a flame of conical shape sitting above the burner lip.

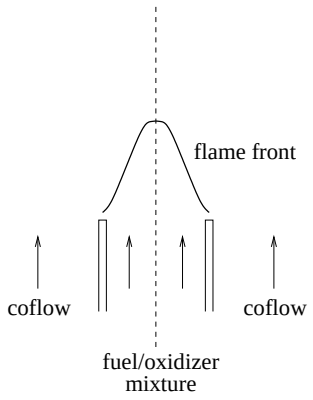

FIG. 1. Schematic of a Bunsen flame.

Since the flow velocity is much smaller than the sound speed, we approximate the fully compressible flow equations using the isobaric flame model [MS85, Wil85, Gio99]. The pressure is split into a thermodynamic part and a spatially varying hydrodynamic perturbation which scales as the square of the Mach number. For through flow problems, the thermodynamic pressure is constant in the computational domain and is specified by the outflow conditions. Density changes only occur because of temperature variations due to strong heat release at the flame front. In

addition, viscous dissipation and hydrodynamic pressure work can be neglected in the energy conservation equation.

The dependent unknowns are written as $u = (Y_1, \dots, Y_{ns}, T, v_1, \dots, v_d, p)$ where $(Y_1, \dots, Y_{ns})$ are the species mass fractions, ns the number of species, T the temperature, $v = (v_1, \dots, v_d)$ the velocity components, d the number of space dimensions and p the hydrodynamic pressure. Let ∂_j denote derivation along the jth spatial coordinate and $\nabla = (\partial_1, \dots, \partial_d)^t$. The governing equations expressed in nonconservative form read

$$\begin{aligned}
e_l(u) &:= (\beta_l \cdot \nabla) Y_l + \nabla \cdot \mathcal{F}_l - \omega_l = 0, \quad 1 \le l \le ns, \\
e_{ns+1}(u) &:= (\beta_{ns+1} \cdot \nabla) T + \nabla \cdot \mathcal{Q} - \omega_T = 0, \\
e_{ns+1+j}(u) &:= (\beta_{ns+1+j} \cdot \nabla) v_j + \partial_j p + (\nabla \cdot \mathcal{V})_j - \rho g_j = 0, \quad 1 \le j \le d, \\
e_{ns+d+2}(u) &:= \nabla \cdot (\rho v) = 0.
\end{aligned} \tag{1}$$

Here, $\mathcal{F}_l$ denotes the mass diffusion flux of the lth species, ω_l its mass production rate, $\mathcal{Q}$ the thermal part of the heat flux, ω_T the temperature source term, $\mathcal{V}$ the viscous stress tensor, $(\nabla \cdot \mathcal{V})_j$ the jth component of its divergence, g_j the jth component of the gravity vector and ρ the density given by the ideal gas law

$$\rho = \frac{p_0 m}{RT}, \tag{2}$$

where p_0 is the thermodynamic pressure, m the mean molecular weight of the mixture given by $m = (\sum_{l=1}^{ns} Y_l / m_l)^{-1}$, m_l the molecular weight of the lth species and R the universal gas constant. The advection velocities β_i, $1 \le i \le ns + d + 1$, are given by $\beta_i = \rho v$ for $i \ne ns + 1$ and $\beta_{ns+1} = \rho c_p v$ where c_p is the mixture specific heat capacity at constant pressure. The species and temperature source terms ω_l and ω_T are given by Arrhenius type expressions and depend exponentially on the temperature. These terms will be detailed in section 5.1.

The multicomponent transport fluxes $\mathcal{F}_l$, $\mathcal{Q}$ and $\mathcal{V}$ read

$$\begin{aligned}
\mathcal{F}_l &= -c_l \nabla Y_l, \quad 1 \le l \le ns - 1, \\
\mathcal{Q} &= -\lambda \nabla T, \\
\mathcal{V} &= -\mu \Big(\nabla v + \nabla v^t - \tfrac{2}{3} (\nabla \cdot v) I \Big),
\end{aligned} \tag{3}$$

while the last species flux ensures overall mass conservation in the form $\sum_{l=1}^{ns} \mathcal{F}_l = 0$. Here, c_l is the diffusion coefficient for the lth species, λ the thermal conductivity and μ the shear viscosity. The expressions in (3) are derived from the kinetic theory of gases with some simplifying assumptions [EG94]. The volume viscosity is not included in the viscous stress tensor since for low Mach flows it can be treated as a perturbation of the hydrodynamic pressure. Furthermore, although Soret and Dufour effects are important in some flame structures [EG98], thermal diffusion coefficients have been neglected for the sake of simplicity. Finally, the mass diffusion fluxes have been taken in the dilution limit in terms of mass fraction gradients. The domain of validity of this assumption is discussed in [EG94, Gio99].

The flame model consists of $nc = ns + d + 2$ coupled nonlinear PDEs equipped with appropriate boundary conditions. In abstract form, its weak formulation reads:

find $u \in V$ such that

$$a(u;\varphi) = 0, \quad \forall \varphi \in V, \tag{4}$$

where V is a suitable subspace of $H^1(\Omega)^{nc}$. Proper modifications of V accounting for essential boundary conditions are not detailed for brevity. We have

$$a(u;\varphi) = \sum_{i=1}^{nc} (r_i^0(u), \varphi_i) + (r_i^1(u), \nabla\varphi_i),$$

with the residual expressions

$$\begin{aligned}
&r_l^0(u) = (\beta_l \cdot \nabla) Y_l - \omega_l && r_l^1 = -\mathcal{F}_l, && 1 \le l \le ns,\\
&r_{ns+1}^0(u) = (\beta_{ns+1} \cdot \nabla) T - \omega_T && r_{ns+1}^1(u) = -\mathcal{Q}, &&\\
&r_{ns+1+j}^0(u) = (\beta_{ns+1+j} \cdot \nabla) v_j + \partial_j p - \rho g_j && r_{ns+1+j}^1(u) = -\mathcal{V}_{j\bullet}, && 1 \le j \le d,\\
&r_{ns+d+2}^0(u) = \nabla \cdot (\rho v) && r_{ns+d+2}^1(u) = 0, &&
\end{aligned} \tag{5}$$

$\mathcal{V}_{j\bullet} \in \mathbb{R}^d$ being the vector with components $(\mathcal{V}_{jj'})_{1 \le j' \le d}$. The form $a(\cdot;\cdot)$ is non-linear with respect to its first argument and linear with respect to the second. Here and in the sequel we use the convention that semi-linear forms are linear with respect to all arguments on the right of the semicolon.

3. STABILIZED FINITE ELEMENT APPROXIMATION

This section describes the stabilized finite element method used to approximate the flame problem and how the discrete equations are solved iteratively.

3.1. Standard Galerkin formulation

Let $\mathcal{T}_h$ denote a conform triangulation of the polygonal computational domain Ω consisting of non-overlapping triangles K. On $\mathcal{T}_h$, we define the finite element space V_h consisting of continuous piecewise affine functions

$$V_h = \{\, \varphi_h \in C^0(\overline{\Omega})^{nc}; \varphi_{h|K} \in P_1(K)^{nc}, \forall K \in \mathcal{T}_h \,\}.$$

Note that the same order of interpolation is used for all physical variables.

In the standard Galerkin approximation, one seeks $u_h \in V_h$ such that

$$a(u_h;\varphi_h) = 0, \quad \forall \varphi_h \in V_h. \tag{6}$$

This method needs to be stabilized in order to cope with (i) advection instabilities due to high Peclet numbers, (ii) pressure-velocity couplings in the low Mach number regime and (iii) spurious oscillations near the flame front causing violation of the discrete maximum principle for the species mass fractions and the temperature. Appropriate stabilizations for the first two effects are rather well known and will only be briefly reviewed. The third effect is less classical in flame modeling and will be discussed in more detail.

3.2. Streamline and pressure-velocity stabilization

For the convection dominated, incompressible Navier-Stokes equations, stable finite element discretizations have been derived using least squares control of the discrete pressure gradient, the incompressibility constraint and the convective derivatives of the dependent variables [BH82, JNP84, Joh87, FF92, TV96]. In this case, energy type stability estimates guarantee the well posedness of the discrete problem. In the low Mach number case, there are no corresponding estimates, but even so the formulation has proved to perform well in several applications [Bra98, BBR99]. The stabilized formulation for low Mach number flames reads: find $u_h \in V_h$ such that

$$a(u_h;\varphi_h) + b^{sd}(u_h;\varphi_h) = 0, \quad \forall \varphi_h \in V_h, \tag{7}$$

with $b^{sd}(u_h;\varphi_h) = \sum_K b_K^{sd}(u_h;\varphi_h)$ and the local stabilizing terms given by

$$\begin{aligned} b_K^{sd}(u_h;\varphi_h) &= \sum_{l=1}^{ns+1} (e_l(u_h), \delta_l^{sd}(\beta_l\cdot\nabla)\varphi_l)_K \\ &+ \sum_{j=ns+2}^{ns+d+1} (e_j(u_h), \delta_j^{sd}(\beta_j\cdot\nabla)\varphi_j + \nabla\varphi_{ns+d+2})_K \\ &+ (e_{ns+d+2}(u_h), \delta_{ns+d+2}^{sd}\nabla\cdot\varphi_v)_K, \end{aligned}$$

with $(\cdot,\cdot)_K$ denoting the $L^2(K)$ inner product. The components of the test function φ_h are denoted by $(\varphi_1,\ldots,\varphi_{ns+d+2})$ and $\varphi_v = (\varphi_{ns+2},\ldots,\varphi_{ns+d+1})$ are the test functions associated with velocity. The stabilization is fully consistent since the exact solution u of (4) also satisfies the approximate problem (7). The stabilizing coefficients are evaluated locally elementwise and given by

$$\delta_i^{sd} = \left(\frac{2|\beta_i|}{h} + \frac{\mu_i}{h^2}\right)^{-1}, \quad 1 \le i \le ns+d+1, \tag{8}$$

and $\delta_{ns+d+2}^{sd} = 4h|\rho v|$. Here, h is the mesh size, $\mu_i = c_i$ for the species, $\mu_{ns+1} = \lambda$ for the temperature and $\mu_{ns+1+j} = \mu$ for the d velocity components.

3.3. Nonlinear crosswind diffusion

Despite its least squares control of streamline derivatives and pressure-velocity coupling, the above method fails to produce a numerical solution satisfying a discrete maximum principle (DMP). More precisely, the species and temperature profiles exhibit minima which sometimes lie significantly below physically acceptable values. This difficulty is particularly severe in combustion problems where negative mass fractions may render the chemistry production terms completely meaningless. In order to quench DMP violations, we introduce an additional stabilization term based on crosswind diffusion (CD). In the literature, such term, also called shock or discontinuity capturing term, has been investigated following two approaches:

- the linear approach where the amount of crosswind diffusion does not depend on the approximate solution. In order to preserve accuracy, the crosswind diffusion scales as $h^{3/2}$. This approach has been introduced in [JSW87] and further extended in [Lub92, SE99];

• the nonlinear approach where the amount of crosswind diffusion depends on the approximate solution. In this context, a new nonlinear crosswind operator has been investigated recently in [BE01]. In particular, for linear advection-diffusion equations discretized on strictly acute meshes, a DMP was rigorously proven.

In the present work, we adapt to flame models the nonlinear approach derived in [BE01] for linear advection-diffusion problems. Nonlinear crosswind diffusion is considered for the temperature and species equations. The fully stabilized Galerkin approximation now reads: find $u_h \in V_h$ such that

$$a(u_h;\varphi_h) + b^{sd}(u_h;\varphi_h) + b^{cd}(u_h;\varphi_h) = 0, \quad \forall \varphi_h \in V_h, \tag{9}$$

with $b^{cd}(u_h;\varphi_h) = \sum_K b_K^{cd}(u_h;\varphi_h)$ and

$$b_K^{cd}(u_h;\varphi) = \sum_{i=1}^{ns+1} ((\beta_i^{\perp}\cdot\nabla)u_{h,i}, \delta_i^{cd}(u_h)(\beta_i^{\perp}\cdot\nabla)\varphi_i)_K,$$

where $u_h = (u_{h,1}, \dots, u_{h,ns+d+2})$. The bilinear form $((\beta_i^{\perp}\cdot\nabla)\cdot, (\beta_i^{\perp}\cdot\nabla)\cdot)$ corresponds to diffusion in the hyperplane orthogonal to the advection vector β_i.

The crosswind diffusion parameter takes the form

$$\delta_i^{cd}(u_h) = \delta_i^{sd} f_i(u_h), \quad 1 \le i \le ns+1,$$

where

$$f_i(u_h) = \min\left(\frac{|e_i(u_h)|}{\left(e_i(u_h)^2 + (\gamma\beta_i^{\perp}\cdot\nabla u_{h,i})^2\right)^{1/2}}, ch^{1/2}\right). \tag{10}$$

All the quantities are evaluated locally elementwise. The numerical parameters γ and c are set to 1 and 0.5 respectively. The nonlinear term in (10) has been considered in [BE01] and is a heuristic simplification of the theoretical crosswind diffusion operator guaranteeing a DMP for linear advection-diffusion problems. The linear term is mainly active at the flame front where nonlinear effects are dominant. Indeed, in regions where the flame front is practically orthogonal to streamlines, we have $\beta_i^{\perp}\cdot\nabla u_{h,i} \ll e_i(u_h)$ and therefore, the nonlinear contribution alone would yield a first order isotropic viscosity resulting in excessive smearing of the flame front. We also point out that the functions $f_i(u_h)$ satisfy two important properties:

• $0 \le f_i(u_h) \le 1$, so that the amount of crosswind diffusion is always lower than that of streamline diffusion;

• $f_i(u_h) = 0$ if $e_i(u_h) = 0$ thus preserving consistency of the discrete problem.

3.4. Newton's method

The discrete flame equations resulting from the stabilized Galerkin formulation (9) read

$$F(U_h) = 0, \tag{11}$$

where $U_h \in \mathbb{R}^{N_h}$ are the nodal components of the discrete solution u_h, N_h is the dimension of V_h and F a nonlinear mapping from $\mathbb{R}^{N_h}$ to $\mathbb{R}^{N_h}$. An approximate solution to (11) is obtained using a damped Newton's method in the form

$$J^k(U_h^{k+1} - U_h^k) = -\lambda^k F(U_h^k),$$

where λ^k is a damping parameter. The matrix $J^k \in \mathbb{R}^{N_h,N_h}$ is an approximation to the Jacobian matrix $\frac{\partial F}{\partial U_h}(U_h^k)$. The matrix J^k is sparse and is computed numerically using perturbed function evaluations. All of its entries, resulting both from spatial and nonlinear local couplings, are retained and stored in compressed form. At each Newton step, the linear system is solved approximately using BiCGStab and a Gauss-Seidel preconditionner blocked at the node level. On structured meshes, larger blocking is also used, e.g., at the row level. Convergence of Newton's method is achieved when the rescaled Euclidean norm of the update vector $U_h^{k+1} - U_h^k$ is less than some prescribed tolerance (typically 10^{-5}).

In order to bring the initial solution estimate into the convergence domain of Newton's method, a time marching algorithm is employed. A discontinuous Galerkin method of degree 0 in time is used resulting in a backward Euler scheme: given u_h^n, find $u_h^{n+1} \in V_h$ such that

$$\begin{aligned}&(u_h^{n+1} - u_h^n, \varphi_h)\\ &+ \tau^n(a(u_h^{n+1};\varphi_h) + b^{sd}(u_h^{n+1};\varphi_h) + b^{cd}(u_h^{n+1};\varphi_h)) = 0, \quad \forall \varphi_h \in V_h,\end{aligned}$$

where τ^n is the time step. These equations are treated in a fully implicit fashion and are solved approximately using Newton's method. For transient iterations, Newton's method generally converges within a couple of iterations.

4. ADAPTIVE MESH GENERATION

Once a numerical solution has been obtained on a given mesh, a key issue is to determine in a *reliable* way whether this solution is acceptable. In other words, one wishes to make sure that the error concerning physical quantities of interest has been brought below a prescribed tolerance. If this is not the case, one also wishes to use the current numerical solution to generate a new computational mesh on which an improved approximation to the exact solution can be obtained. The dual weighted residual method offers a suitable theoretical framework to achieve these goals. In this section, we highlight the main ideas underlying the method and discuss its practical implementation in the context of flame problems.

4.1. The dual weighted residual method

The dual weighted residual method uses nonlinear optimal control techniques to estimate a given functional of the numerical error in terms of local residuals of the approximate solution. The residuals are weighted by coefficients resulting from a linearized dual problem providing information on where the error is actually generated. We refer to [BR01] for a recent review of the theoretical framework with various numerical examples.

Let $\Psi(\cdot)$ be a user specified functional defined on the solution space V representing some quantity of physical interest, e.g. in combustion applications, fuel

mass fraction, temperature or a pollutant flux averaged over a region where measurements are performed. We assume that the functional J is differentiable and denote by $\Psi'(\cdot\,;\cdot)$ its derivative. Similarly, for a semi-linear form $a(\cdot\,;\cdot)$ which is differentiable with respect to its first argument, we denote by $a'(\cdot\,;\cdot,\cdot)$ its derivative.

We present the dual weighted residual method in an abstract setting and will discuss the validity of the assumptions for flame problems further below. We assume that the continuous problem (4) and the discrete problem (9) are well posed (at least locally). Let u and u_h denote their respective solutions and let $e = u - u_h$ be the error. We introduce the fully stabilized semi-linear form $a_{sd/cd}(\cdot\,;\cdot) = a(\cdot\,;\cdot) + b^{sd}(\cdot\,;\cdot) + b^{cd}(\cdot\,;\cdot)$ and assume that

(h1) the semi-linear form $a_{sd/cd}(\cdot\,;\cdot)$ is differentiable.

We then introduce the linearized dual problem: find $z \in V$ such that

$$\int_0^1 a'_{sd/cd}(u_h + se; \varphi, z)\,\mathrm{ds} = \int_0^1 \Psi'(u_h + se; \varphi)\,\mathrm{ds}, \quad \forall \varphi \in V, \tag{12}$$

and assume that

(h2) the linearized dual problem (12) is well posed.

In order to obtain an error representation in terms of the dual problem (12), we assume that

(h3) the discrete problem (9) is consistent, i.e., the exact solution u of (4) satisfies $a_{sd/cd}(u; \varphi_h) = 0$, $\forall \varphi_h \in V_h$.

These assumptions lead to the following result [BR01].

PROPOSITION 4.1. *Assuming* **(h1)**–**(h3)**, *we have the error representation*

$$\Psi(u) - \Psi(u_h) = \min_{\varphi_h \in V_h} a_{sd/cd}(u_h; z - \varphi_h), \tag{13}$$

where z is the solution of the linearized dual problem (12).

We next split the right member of (13) as a sum over the mesh triangles of a local residual of the approximate solution u_h weighted by a coefficient depending on the local regularity of the dual solution z. To this purpose, we make the following two assumptions:

(h4) the finite element space V_h has optimal interpolation properties: there exists a dense subspace W of V with a local seminorm $|\cdot|_{W,K}$, an interpolation constant c_i and an interpolation operator $i_h : W \to V_h$ such that

$$\begin{cases} \forall w \in W,\ \forall h,\ \forall K \in \mathcal{T}_h, \\ \|w - i_h w\|_K + h_K \|\nabla(w - i_h w)\|_K + h_K^{1/2} \|w - i_h w\|_{\partial K} \le c_i\, h_K^2 |w|_{W,K}, \end{cases} \tag{14}$$

where ∂K is the boundary of K;

(h5) the solution of the linearized dual problem (12) is in W.

PROPOSITION 4.2. *Assume* **(h1)**–**(h5)**. *For* $1 \leq l \leq nc$ *and* $K \in \mathcal{T}_h$, *define the weights*

$$\omega_K^l = c_i \, h_K \, |z_l|_{W,K}, \tag{15}$$

where $z = (z_1, \ldots, z_{nc})$ *is the solution of the linearized dual problem (12). We then have the a posteriori error estimate*

$$|\Psi(u) - \Psi(u_h)| \leq \sum_{K \in \mathcal{T}_h} \left(\mathcal{E}_K^0 + \mathcal{E}_K^1 + \mathcal{E}_K^{sd} + \mathcal{E}_K^{cd} \right), \tag{16}$$

with

$$\begin{cases} \mathcal{E}_K^0 = \displaystyle\sum_{l=1}^{ns+d+2} h_K \, \|e_l(u_h)\|_K \, \omega_K^l \\ \mathcal{E}_K^1 = \displaystyle\sum_{l=1}^{ns+d+1} h_K^{1/2} \, \| \, [r_l^1(u_h)] \, \|_{\partial K} \, \omega_K^l \\ \mathcal{E}_K^{sd} = \displaystyle\sum_{l=1}^{ns+d+1} \tfrac{1}{2} h_K \, \|e_l(u_h)\|_K \, \omega_K^l + \sum_{j=1}^{d} h_K \, c_K \|e_{ns+j+1}(u_h)\|_K \omega_K^{ns+d+2} \\ \qquad\qquad + h_K \, c_K' \|e_{ns+d+2}(u_h)\|_K \displaystyle\sum_{j=1}^{d} \omega_K^{ns+j+1} \\ \mathcal{E}_K^{cd} = \displaystyle\sum_{l=1}^{ns+1} \tfrac{1}{2} h_K \, \|(\beta_l^\perp \cdot \nabla) u_{h,l}\|_K \, \omega_K^l \end{cases}$$

where $[\cdot]$ *is the jump across* ∂K, $c_K = 1/(2|\rho_h v_h|_K + \mu/h_K)$, ρ_h *and* v_h *are the discrete density and velocity evaluated from* u_h *and* $c_K' = 4|\rho_h v_h|_K$.

Proof. Upon choosing $\varphi_h = i_h z$ in (13), splitting integrals over elements, integrating by parts the first order residuals $r_l^1(u_h)$ and using the interpolation inequality (14), the standard Galerkin part $a(u_h, z - i_h z)$ is readily estimated by $\sum_{K \in \mathcal{T}_h} (\mathcal{E}_K^0 + \mathcal{E}_K^1)$. On the other hand, using (8) we get $\delta_i^{sd} h / \beta_i \leq \frac{1}{2}$. Therefore, owing to the fact that the CD operator is such that $f_i(u_h) \leq 1$, the stabilizing terms $b^{sd}(u_h, z - i_h z)$ and $b^{cd}(u_h, z - i_h z)$ are readily estimated by $\sum_{K \in \mathcal{T}_h} (\mathcal{E}_K^{sd} + \mathcal{E}_K^{cd})$. ■

The validity of assumptions **(h1)**–**(h5)** in the context of flame modeling requires some discussion. **(h4)** is a classical property of finite element interpolation valid for instance on regular meshes with the Sobolev space $W = H^2(\Omega)$ and $|w|_{W,K} = (\sum_{1 \leq j \leq j' \leq d} \|\partial_{jj'} w\|_K^2)^{1/2}$. **(h3)** is also satisfied since both streamline and crosswind diffusion terms vanish for the exact solution. Concerning **(h1)**, one potential difficulty is the use of absolute values in the stabilizing coefficients. However, such singularities often occur in regions of low physical interest and should have a minor impact on the error estimator. Absolute values can also be regularized. Assumptions **(h2)** and **(h5)** are more difficult to establish mathematically since the adjoint solution z may only exist in a weak sense. Nevertheless this is not too critical since in practical implementations one considers a finite dimensional approximate dual problem and its solution usually exhibits more regularity. In ad-

dition, the discrete dual problem may be interpreted as a stabilized approximation of a formal dual problem.

Finally, we point out that for first degree polynomial interpolation and constant diffusion coefficients, the quantities $e_l(u_h)$ can be replaced by $r_l^0(u_h)$ in the error indicator $\mathcal{E}_K^0$. Furthermore, the residual terms should be dominated by the jump terms $\mathcal{E}_K^1$ [CV99, BR01]. The stabilizing contributions $\mathcal{E}_K^{sd}$ and $\mathcal{E}_K^{cd}$ should also be small at least on the finer meshes. These issues will be further investigated in section 5.

4.2. Practical implementation

Concessions to practicality need to be made in order to use the theoretical results of section 4.1 for adaptive mesh generation in combustion applications.

Owing to the nonlinear character of the original problem (4), the linearized dual problem (12) depends on the exact solution u. Therefore, we consider the following approximate dual problem: find $\tilde{z} \in V$ such that

$$a'_{sd/cd}(u_h; \varphi, \tilde{z}) = \Psi'(u_h; \varphi), \quad \forall \varphi \in V, \tag{17}$$

which results from (12) by using the approximate quadrature $\int_0^1 f(s)\,\mathrm{d}s \simeq f(0)$. An error representation can also be obtained directly from the dual problem (17) [BR01]. It involves the minimal residual as in (13) plus a remainder term which is quadratic in the error. This term may be viewed as a measure of the nonlinearities of the problem and should be small whenever the approximate solution u_h is close to the exact solution u.

Since (17) is posed in the infinite dimensional space V, we need to consider a discrete version of the approximate dual problem. The simplest approach is to use a Galerkin method on V_h so that we now seek $\tilde{z}_h \in V_h$ such that

$$a'_{sd/cd}(u_h; \varphi_h, \tilde{z}_h) = \Psi'(u_h; \varphi_h), \quad \forall \varphi_h \in V_h. \tag{18}$$

More elaborate strategies include considering approximations to $\tilde{z}$ obtained by a higher order method or on a finer mesh and are discussed for instance in [BR01]. The present approach offers the advantage that it does not increase memory size requirements which in combustion problems are already at high demand. Another advantage of (18) is that the transpose of last Jacobian used in Newton's method can be used as stiffness matrix in (18).

Second order derivatives of the approximate dual solution $\tilde{z}_h$ need to be evaluated in order to compute the weights ω_K^l in (15). These quantities are approximated by second-order divided difference quotients $D_{jj'}^h \tilde{z}_h$, $1 \le j, j' \le d$. The a posteriori error estimate (16) is thus used with the approximate weights

$$\tilde{\omega}_{hK}^l = h_K^2 \left(\sum_{1 \le j \le j' \le d} (D_{jj'}^h \tilde{z}_{h,l})^2 \right)^{1/2}, \tag{19}$$

the interpolation constant c_i being estimated by 1 (which is generally an upper bound).

The adaptive solution algorithm reads:

(A) chose an initial coarse mesh $\mathcal{T}_{(0)}$. Set $i = 0$;

(B) solve the approximate flame problem (9) on $\mathcal{T}_{(i)}$. Let $u_{(i)}$ be the solution;

(C) solve the approximate dual problem (18) and evaluate the approximate weights (19). Compute the local error indicators $\mathcal{E}_K^0$, $\mathcal{E}_K^1$, $\mathcal{E}_K^{sd}$ and $\mathcal{E}_K^{cd}$;

(D) if the global error $\sum_{K\in\mathcal{T}_{(i)}}(\mathcal{E}_K^0 + \mathcal{E}_K^1 + \mathcal{E}_K^{sd} + \mathcal{E}_K^{cd})$ is below a prescribed tolerance TOL, stop; otherwise, use the local error indicators to generate a new mesh $\mathcal{T}_{(i+1)}$, set $i := i + 1$ and go back to step (B).

Several methods can be designed to generate the new mesh $\mathcal{T}_{(i+1)}$ depending on the type of data structure considered:

- locally refined triangulations: starting from an initial triangulation derived from a tensor product mesh of quadrangles of size h_0, such meshes consist of triangles belonging to quadrangles of size $2^{-p}h_0$, $0 \le p \le P$, where P is the number of local refinements already performed. In locally refined triangulations, the local error indicators are conveniently evaluated on the underlying quadrangles which are marked for refinement or derefinement by equidistributing the error indicators;
- fully unstructured triangulations: the local error indicators are evaluated on the triangles and are used to define a control function specifying the desired mesh size $h(x)$ locally. This function, in turn, can be used as input for a Delaunay mesh generator.

In the next section, we present numerical results for both locally refined and fully unstructured triangulations.

5. NUMERICAL RESULTS

We apply the numerical methods described in the previous sections to a methane/air Bunsen flame in axisymmetric configuration (see figure 1). We first specify the chemical model and the boundary conditions. We then study numerically the adaptive algorithm based on a posteriori error estimates and investigate the impact of nonlinear crosswind diffusion on numerical results. Solution quality is assessed in terms of overall flame characteristics, including height, lift off and width and also in terms of undershoots in species and temperature profiles.

5.1. The Bunsen flame problem

The flame is obtained by flowing a stoichiometric methane/air mixture through a cylindrical tube. The fuel tube has a radius of 4 mm and a width of 0.5 mm. The inflow velocity profile is parabolic with a peak velocity of 1.5 m/s. The flame is surrounded by an air coflow given by $v_z^{\rm cfl}(r) = v_0(1 - \exp(-(r - r_0)/\delta))$ with peak velocity $v_0 = 1$ m/s and parameters $r_0 = 4.5$ mm and $\delta = 2$ mm. Reactants and air are flown at room temperature (298 K).

We consider a simplified chemistry model [CKM83] based on the overall reaction

$$\mathrm{CH_4} + 2\mathrm{O_2} \rightarrow \mathrm{CO_2} + 2\mathrm{H_2O}.$$

Three species mass fractions are retained among the dependent unknowns, namely $Y_{\mathrm{CH_4}}$, $Y_{\mathrm{O_2}}$ and $Y_{\rm prod}$, the latter associated with the combustion products. Nitrogen is also present in the mixture as an inert dilutant. Its mass fraction is conveniently evaluated from $Y_{\mathrm{N_2}} = 1 - Y_{\mathrm{CH_4}} - Y_{\mathrm{O_2}} - Y_{\rm prod}$.

The mixture specific heat capacity is assumed to be constant and equal to $c_{pm} = 0.323$ cal/g/K. The energy conservation equation is rescaled by c_{pm}. The temperature source term then reads

$$\omega_T = \frac{Q}{c_{pm}} E(\rho, Y_1, ..., Y_{ns}, T),$$

where we have introduced

$$E(\rho, Y_1, ..., Y_{ns}, T) = (\rho Y_{\mathrm{CH_4}}) (\rho Y_{\mathrm{O_2}})^2 A_{ar} \exp(-E_{ar}/(R_{uc}T)),$$

with $Q = 11355$ cal/g, $A_{ar} = 1.01 \cdot 10^{18}$ (cgs units), $E_{ar} = 29100$ cal/mol and $R_{uc} = 1.9872$ cal/mol/K. On the other hand, the species source terms are given by

$$\omega_l = \tilde{m}_l E(\rho, Y_1, ..., Y_{ns}, T), \quad 1 \leq l \leq 3,$$

with $\tilde{m}_1 = -1$, $\tilde{m}_2 = -2m_{\mathrm{O_2}}/m_{\mathrm{CH_4}}$, $\tilde{m}_3 = m_{\mathrm{prod}}/m_{\mathrm{CH_4}}$ and $m_{\mathrm{prod}} = 2m_{\mathrm{H_2O}} + m_{\mathrm{CO_2}}$. The molecular weights are $m_{\mathrm{CH_4}} = 16.043$, $m_{\mathrm{O_2}} = 31.9988$, $m_{\mathrm{CO_2}} = 44.01$, $m_{\mathrm{H_2O}} = 18.0153$ and $m_{\mathrm{N_2}} = 28.0134$ in g/mol. Finally, the thermal conductivity is given by $\lambda = R_l/(\rho c_{pm})$ with $R_l = 5.61 \cdot 10^{-8}$ (cgs units), the shear viscosity by $\mu = P_r \lambda$ with $P_r = 0.7$ and the species diffusion coefficients by $c_i = \lambda/(\rho Le_i)$ with the Lewis numbers set to $Le_{\mathrm{CH_4}} = 0.96$, $Le_{\mathrm{O_2}} = 1.1$ and $Le_{\mathrm{prod}} = 0.83$.

Boundary conditions are as follows:

- inflow ($z = 0$): Dirichlet for both velocity components and temperature, flux condition for the species in the form

$$\rho Y_l v_z + \mathcal{F}_l \cdot e_z = \rho^{\mathrm{in}} v_z^{\mathrm{in}} Y_l^{\mathrm{in}}, \quad 1 \leq l \leq 3,$$

where the superscript denotes inflow conditions and e_z the upward unit vector. For stoichiometric methane/air flames, we have $Y_{\mathrm{CH_4}}^{\mathrm{in}} = 0.05515$ and $Y_{\mathrm{O_2}}^{\mathrm{in}} = 0.22$;

- outflow ($z = Z$): homogeneous Dirichlet for hydrodynamic pressure and radial velocity, homogeneous Neumann for axial velocity, temperature and species;

- axis of symmetry and far field ($r = 0$ and $r = R$): homogeneous Dirichlet for radial velocity, homogeneous Neumann for axial velocity, temperature and species.

All the results reported below have been obtained on the computational domain $[0, 3] \times [0, 25]$ in cm.

5.2. The adaptive algorithm

In this section we investigate numerically the adaptive algorithm discussed in section 4.2. For the sake of illustration, we have chosen to control the mean error in methane mass fraction

$$\Psi(u) = \int_\omega Y_{\mathrm{CH_4}} \mathrm{d}x. \tag{20}$$

The control domain is set to $\omega = [0, 1] \times [0, 1]$ in cm and covers the entire flame region since flame lengths are typically 0.9 cm for the present operating conditions.

Other error functionals may be easily selected depending on the user's specific requirements. The tolerance for the adaptive algorithm was set to TOL = 10^{-3}. The adaptive algorithm was started from a coarse initial mesh of locally refined type. This mesh, referred to as level 0, contained 895 nodes and 1617 triangles with 20 elements of size 0.25 mm (half the tube width) located around the burner lip and a maximal element size of 0.4 cm (see figure 2). To bring the error below the tolerance threshold, three adaptive refinement steps were needed. The corresponding locally refined meshes will be referred to as level 1, 2 and 3. We then refined an additional level to obtain a reference solution permitting us to compare the a posteriori error estimate with the error between the reference solution and a given numerical approximation. Locally refined meshes at levels 2 and 4 are also shown in figure 2.

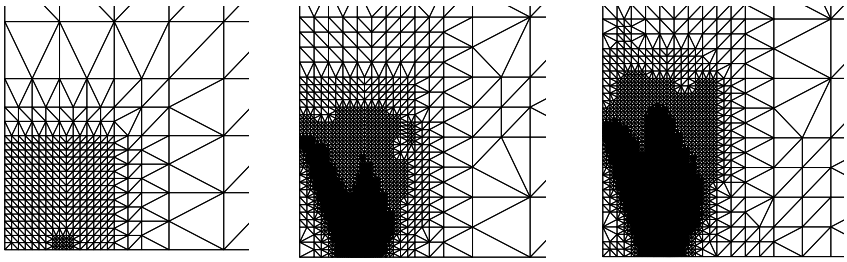

FIG. 2. Examples of locally refined meshes at levels 0, 2 and 4

The adaptive algorithm has also been investigated on fully unstructured triangulations. Such meshes are of Delaunay type and have been generated using the algorithm described in [Reb93]. On a given refinement level, the interior control function specifying the desired element size has been obtained from the a posteriori error estimates computed on the locally refined mesh where second order derivatives are easier to evaluate. Fully unstructured triangulations at levels 0, 2 and 4 are illustrated in figure 3.

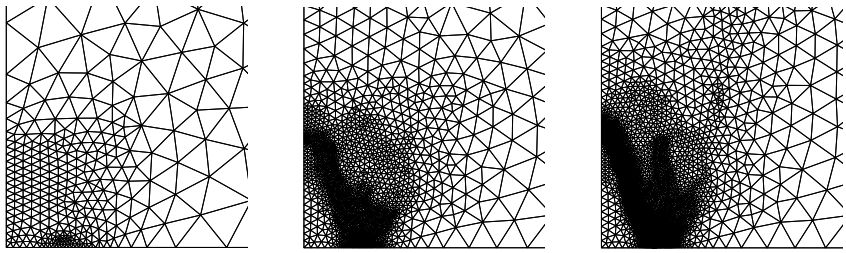

FIG. 3. Examples of fully unstructured meshes at levels 0, 2 and 4

The number of degrees of freedom for all the meshes considered is reported in table 1. For high refinement levels, fully unstructured meshes result in less degrees of freedom than locally refined ones (the ratio is more than two on level 4) because the equilateral triangles in the Delaunay meshes appear to cover the computational

domain more efficiently and because of the sharper transition to the outer coarse mesh in the fully unstructured case.

TABLE 1
Number of nodes for the locally refined and the fully unstructured meshes at various refinement levels

level	0	1	2	3	4
locally refined	895	1694	3568	7728	16570
fully unstructured	839	1337	2155	4338	7257

The numerical solution of the approximate dual problem (18) obtained on the locally refined mesh of level 0 is presented in figure 4. We consider the components associated with methane, temperature, axial velocity and pressure. Although the data for the dual problem is nonzero for methane only, all the physical components of the dual solution are important because of the strongly coupled nature of the flame problem. In particular, refinement of the flame front is mainly driven by temperature and pressure on coarser meshes while velocity components are active above the burner lip where the flow has stagnation points. The methane component is also active in the shear flow layer outside the flame developing from the hydrodynamic interaction between the jet flow and the air coflow. In figure 5 we show the dual solution for level 3. We observe that the dual solution profiles have become much smoother indicating that the theoretical assumptions **(h2)** and **(h5)** are reasonable as higher resolution is achieved.

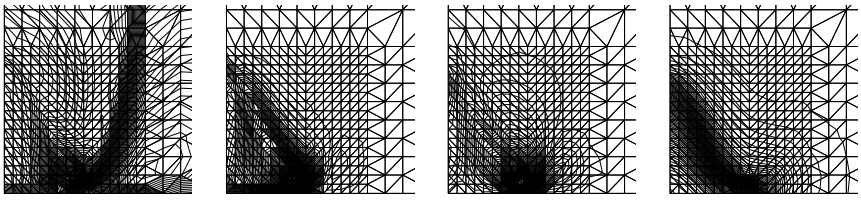

FIG. 4. Dual solution on locally refined mesh of level 0; from left to right: methane, temperature, axial velocity and pressure

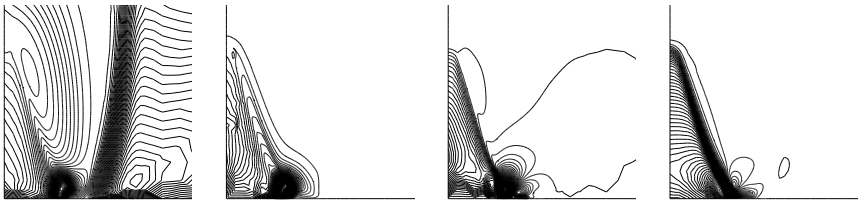

FIG. 5. Dual solution on locally refined mesh of level 3; from left to right: methane, temperature, axial velocity and pressure

The a posteriori error estimate is presented in figure 6 as a function of the total number of degrees of freedom N for the locally refined meshes. Similar results are obtained for the fully unstructured meshes. The overall convergence rate scales as $N^{-3/2}$. Since N is inversely proportional to $h_{\min}$, the lowest mesh size, we deduce that the error indicator decreases as $h_{\min}^{3/2}$ in agreement with theoretical estimates valid for simpler problems. In figure 6 we also report estimates of the mean error and the L^1 error obtained using the numerical solution on level 4 as a reference. Denoting by $u_{(4)}$ this reference solution, we plot the quantities $|\int_\omega u_{(4)} - u_{(i)}|$ and $\int_\omega |u_{(4)} - u_{(i)}|$ for $0 \leq i \leq 3$. We observe that the a posteriori error estimate nevers underpredicts the error. The estimate also appears to be rather sharp since the ratio between the a posteriori estimate and the L^1 error is only 1.3 on level 3. Moreover, we note that the mean error and the L^1 error are very similar, thus indicating that the error is globally of the same sign over the control domain ω. Finally, we point out that the three error estimates exhibit a similar convergence rate on finer meshes.

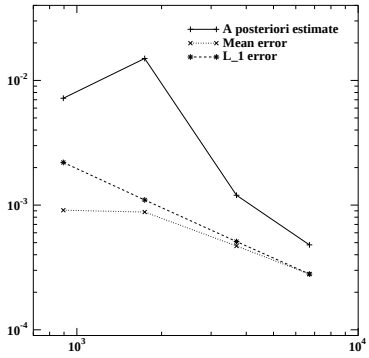

FIG. 6. A posteriori error estimate as a function of total degrees of freedom on locally refined meshes; comparison with the mean error and the L^1 error evaluated using the numerical solution on level 4 as reference

In figure 7 we plot the relative contribution from the different error terms to the a posteriori error estimate. On finer meshes, the term corresponding to the jump in the gradients, $\mathcal{E}_K^1$, dominates the error estimate. This result is in agreement with theoretical estimates [CV99, BR01]. A significant contribution to this term arises near the burner lip where the inflow velocity profile exhibits discontinuous normal derivatives. We also point out that the streamline diffusion contribution, $\mathcal{E}_K^{sd}$, is half the lower order residual contribution, $\mathcal{E}_K^0$, while the crosswind diffusion contribution, $\mathcal{E}_K^{cd}$, is approximately an order of magnitude smaller than the others on all meshes.

Finally, we present in figure 8 contours for temperature, methane, velocity norm and pressure obtained from the reference solution on level 4. For each physical component we compare the locally refined and fully unstructured results and observe very good agreement.

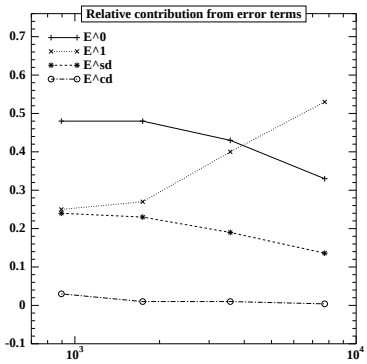

FIG. 7. Relative contribution of error indicators $\mathcal{E}_K^0$, $\mathcal{E}_K^1$, $\mathcal{E}_K^{sd}$ and $\mathcal{E}_K^{cd}$ as a function of total degrees of freedom on locally refined meshes

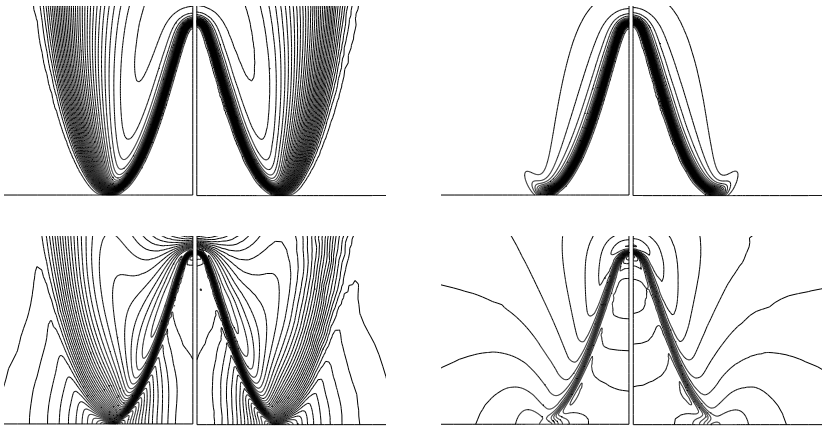

FIG. 8. Comparison of the reference flame solution obtained on the locally refined (left) and fully unstructured (right) meshes of level 4; from top left to bottom right: temperature, methane, velocity norm and pressure

5.3. Impact of crosswind diffusion on solution quality

The numerical results presented in the previous section have been obtained using the nonlinear CD operator (10) presented in section 3.3. As already pointed out in section 3.2, the stabilization for pressure-velocity coupling is based on the implicit assumption that the flow locally has the same stability properties as the incompressible Navier-Stokes equations. This assumption is clearly not valid near the flame front where the density undergoes significant changes. A mathematical study of pressure-velocity stabilization with strong density gradients is beyond the scope of this paper. To avoid pressure oscillations and smooth the velocity field in zones with strong underresolved temperature gradients, a linear CD operator is always considered for the momentum equations. To preserve accuracy, such term scales as $h^{3/2}$. With this modification, the semi-linear form $b^{cd}(\cdot\,;\cdot) = 0$ is no longer

TABLE 2
Flame height computed on various meshes

mesh	locally refined			fully unstructured		
method	SD	linear	nonlinear	SD	linear	nonlinear
level 0	0.77	0.70	0.74	—	0.64	0.5
level 1	0.86	0.83	0.85	0.87	0.79	0.83
level 2	0.89	0.87	0.88	0.88	0.85	0.87
level 3	0.89	0.89	0.89	0.90	0.89	0.89
level 4	0.89	0.88	0.89	0.90	0.89	0.90

consistent but its contribution to the a posteriori estimate is expected to be small at least on finer meshes.

In order to investigate the impact of CD on solution quality, we compare the numerical solutions obtained from 3 sets of results labelled as follows:

- SD: no CD stabilization, simply $f_i(u_h) = 0$ for $1 \leq i \leq ns + 1$;
- linear: $f_i(u_h) = ch^{1/2}$ with $c = 0.5$ for $1 \leq i \leq ns + 1$;
- nonlinear: $f_i(u_h)$ given by (10) for $1 \leq i \leq ns + 1$.

On coarser meshes, CD stabilization is critical in improving convergence rates. The SD method failed to converge on the fully unstructured mesh of level 0, with a temperature undershoot in the Newton iterates of 168 K. Before further discussion of computational costs, we investigate solution quality. We consider first overall flame characteristics such as height, lift off and width and then undershoots in species and temperature profiles.

Flame heights, defined as point on the z-axis where half of the injected combustible has been consumed, are reported in table 2. On level 4, all the numerical solutions agree within 0.1 mm, i.e., within 1%, independently of the type of mesh and CD operator. However, important fluctuations due to the underresolution are observed on coarse meshes. As expected, CD methods yield shorter flames than the SD method on coarse meshes because upstream flame propagation is enhanced by diffusion so that more diffusive flames stabilize closer to the premixed fuel jet. The flame lift off, defined as the lowest z-coordinate where the temperature reaches 1000 K, is presented in table 3. Conclusions are similar to those drawn for the flame height. We note however a much stronger sensitivity to flame resolution, the ratio between lift off at level 0 and 4 being roughly 3. In table 4, we consider the radial flame width at $z = 0.4$ mm. Drawing a horizontal line at $z = 0.4$ mm, we denote by $x^l_{10\%}$ the position on the left side of the flame where the heat production reaches ten percent of its maximum value and by $x^r_{10\%}$ the corresponding point on the right side. The flame width is then evaluated as $x^r_{10\%} - x^l_{10\%}$. On coarse meshes, flame width is expected to be larger when CD is included, but on level 4 flame widths agree to within a few percent.

Figure 9 compares temperature profiles computed on fully unstructured meshes at levels 1 and 2. Left plots are obtained with nonlinear CD and right ones with SD only. On level 1, the SD method predicts a flame front with a somewhat irregular shape near the flame tip whereas the nonlinear CD method yields a more conical

TABLE 3
Flame lift off computed on various meshes

mesh	locally refined			fully unstructured		
method	SD	linear	nonlinear	SD	linear	nonlinear
level 0	0.072	0.085	0.080	—	0.047	0.095
level 1	0.043	0.048	0.044	0.044	0.067	0.047
level 2	0.031	0.031	0.031	0.032	0.033	0.032
level 3	0.026	0.027	0.027	0.027	0.028	0.027
level 4	0.024	0.024	0.025	0.026	0.026	0.026

TABLE 4
Radial flame width at $z = 4$ mm computed on various meshes

mesh	locally refined			fully unstructured		
method	SD	linear	nonlinear	SD	linear	nonlinear
level 0	0.077	0.088	0.075	—	0.11	0.11
level 1	0.049	0.051	0.052	0.064	0.084	0.064
level 2	0.052	0.052	0.052	0.056	0.059	0.057
level 3	0.051	0.050	0.051	0.053	0.052	0.050
level 4	0.052	0.051	0.052	0.053	0.051	0.053

shape. On level 2, both methods capture a similar shape for the flame front. We also observe how the flames move closer to the burner lip as resolution is improved.

We next study how well the different CD operators handle undershoots in the solution. In figure 10 we present the maximal undershoot for temperature and methane as a function of the total number of degrees of freedom on the locally refined meshes. The methane undershoot is quenched as soon as the mesh is refined. This result is coherent with the present choice of the error functional where methane is the targeted quantity. On the other hand, temperature undershoots at physically unacceptable values persist with the SD method even on finer meshes. Undershoots for temperature, methane and product obtained from the three CD operators on all meshes are reported in tables 5–7. For fully unstructured meshes on level 0, significant temperature undershoots are present even with CD stabilization, a phenomenon not observed for locally refined meshes. Temperature undershoots are quenched at level 2 or 3 depending on the type of mesh. For methane, the linear and nonlinear CD operators yield similar results while the nonlinear one appears to be more effective to wipe out product undershoots.

The geometric location of temperature undershoots is presented in figure 11 (left) for the solution obtained with nonlinear CD on the locally refined mesh of level 4. The undershoots, 1 K in magnitude, are present both in the flame front and in the shear layer between inner and outer jets. Figure 11 (right) shows which contribution to the minimum in equation (10) is active with black corresponding to the linear one. As expected, the nonlinear contribution is mainly active in the convective layer outside the flame while the $h^{3/2}$ term dominates in most triangles covering the flame front. The linear CD method is too diffusive in the downstream region

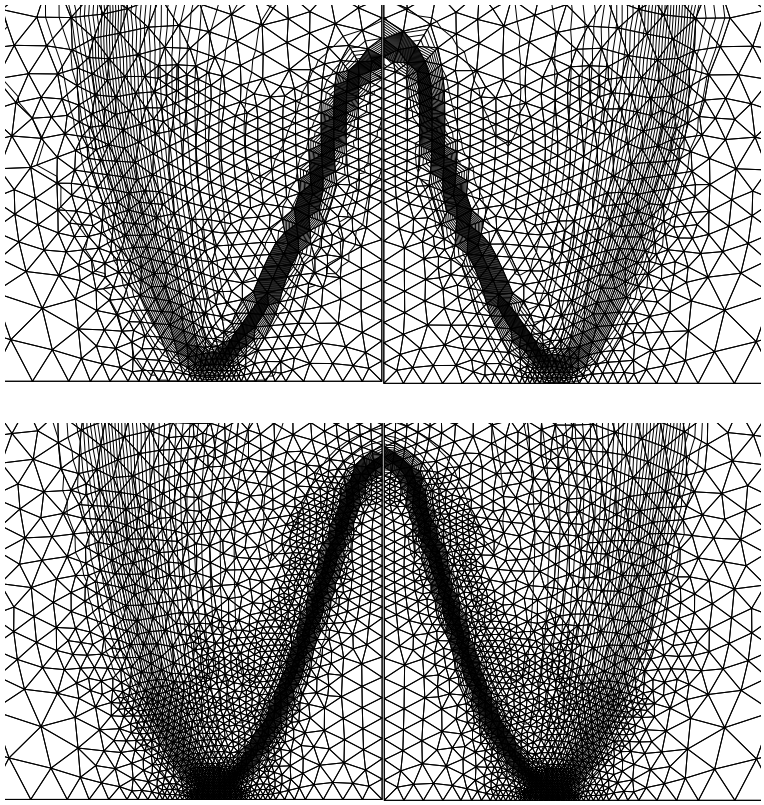

FIG. 9. Comparison of computed temperature on fully unstructured meshes of level 1 (top) and level 2 (bottom) using the nonlinear CD operator (left) and the simple SD method (right).

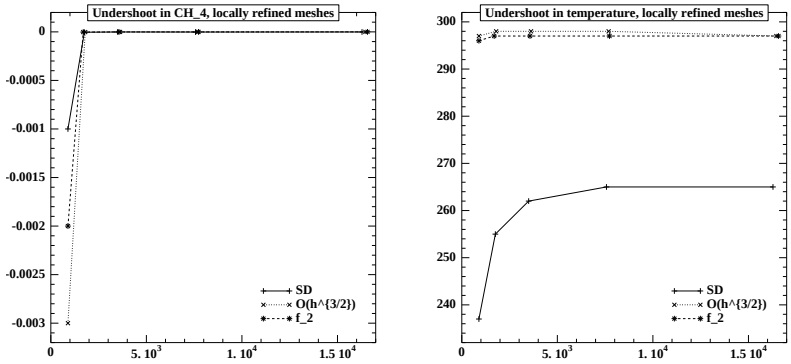

FIG. 10. Undershoots for different methods as a function of total degrees of freedom; left: methane, right: temperature; locally refined meshes

and results in excessive smearing of the temperature profile. On the other hand,

TABLE 5
Temperature undershoots computed on various meshes

mesh	locally refined			fully unstructured		
method	SD	linear	nonlinear	SD	linear	nonlinear
level 0	237	297	296	—	256	277
level 1	255	298	297	239	280	271
level 2	262	298	297	258	292	293
level 3	265	298	297	255	297	297
level 4	265	297	297	268	298	297

TABLE 6
Methane undershoots computed on various meshes

mesh	locally refined			fully unstructured		
method	SD	linear	nonlinear	SD	linear	nonlinear
level 0	-0.001	-0.003	-0.002	—	-0.0029	-0.0045
level 1	-3.8 E-6	-2.4 E-6	-2.2 E-6	-1.3 E-5	-4.6 E-6	-2.6 E-6
level 2	-1.2 E-6	-7.6 E-7	-7.4 E-7	-1.1 E-6	-7.9 E-7	-4.2 E-7
level 3	-1.7 E-6	-6.3 E-7	-2.6 E-7	-7.2 E-7	-1.3 E-7	-2.1 E-7
level 4	-1.1 E-6	-3.0 E-7	-1.3 E-7	-6.2 E-7	-1.4 E-7	-2.6 E-7

TABLE 7
Product undershoots computed on various meshes

mesh	locally refined			fully unstructured		
method	SD	linear	nonlinear	SD	linear	nonlinear
level 0	-0.009	-0.0001	-0.0003	—	-0.012	-0.0029
level 1	-0.006	-0.0005	-7.8 E-5	-0.008	-0.0055	-0.0026
level 2	-0.005	-0.0001	-6.6 E-5	-0.005	-0.0030	-0.00047
level 3	-0.005	-0.0002	-2.5 E-5	-0.005	-0.0012	-0.0001
level 4	-0.005	-0.0002	-7.2 E-5	-0.004	-0.0002	-8.7 E-5

the nonlinear CD method offers a reasonable compromise between resolution of the downstream thermal layer and undershoot quenching.

We finally assess the computational overhead associated with CD operators, linear or nonlinear. To this purpose, we use the SD solution on level 2 as an initial estimate to obtain a converged solution with linear or nonlinear CD. We take 75 time steps and then solve the stationary system. Table 8 reports the total number of Jacobian evaluations and the linear algebra cost. The latter is estimated as the number of BiCGStab iterations times the square of the total degrees of freedom and is normalized by the linear algebra cost for achieving convergence with the SD method on the locally refined mesh of level 2 starting from the converged solution on level 1. On locally refined meshes, the linear algebra overhead of the nonlinear method is significant but is only slightly higher than that of the linear method on

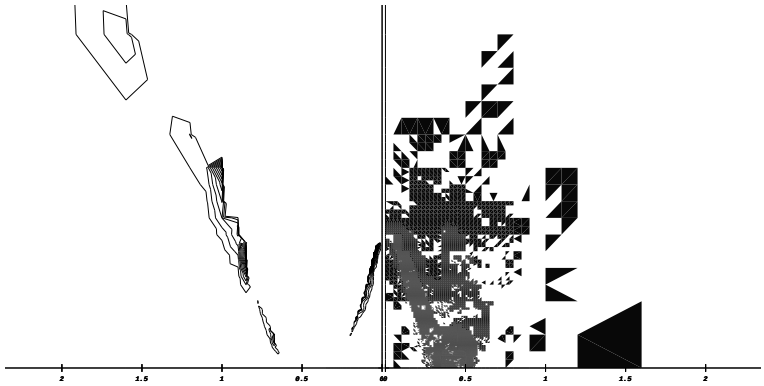

FIG. 11. Locally refined mesh of level 4; left: regions where the temperature exhibits an undershoot of 1 K; right: the linear CD operator dominates the nonlinear term in the black zone

fully unstructured meshes. On the other hand, the total number of Jacobians is comparable for all cases, although their evaluation is cheaper on fully unstructured meshes which have less degrees of freedom than locally refined ones.

TABLE 8

Comparison of computational cost for linear and nonlinear CD

mesh type	locally refined		fully unstructured	
method	linear	nonlinear	linear	nonlinear
Jacobians	76	83	80	85
linear algebra cost	1.22	2.56	0.74	0.87

6. CONCLUSIONS

In this paper we derived a stabilized finite element discretization for low Mach, steady, laminar flames. The adaptive mesh methodology relies on the dual weighted residual method. We presented an abstract analysis of the method including SD and CD contributions to the error indicators and discussed the validity of the underlying assumptions for flame problems. Numerical results have been presented for a stoichiometric methane/air Bunsen flame with simple chemistry. The adaptive algorithm performs well on both locally refined and fully unstructured meshes, the latter achieving similar accuracy with less degrees of freedom. In addition, various CD operators have been compared in terms of solution quality and computational costs. The SD method without any CD stabilization produces physically unacceptable temperature undershoots and has severe convergence difficulties especially on coarse, fully unstructured meshes. Linear and nonlinear CD methods yield similar results in terms of solution quality, the latter being more expensive on locally refined meshes but yielding a sharper resolution of the downstream thermal layer. Forthcoming work includes extension of the present methodology to finite rate kinetics and further investigation of least squares control for low Mach flows.

ACKNOWLEDGMENT

The first author gratefully acknowledges financial support from the Hans Werthen foundation, the Swedish Foundation for International Cooperation in Research and Higher Education and Ecole Polytechnique, France.

REFERENCES

BBR99

BBR99. R. Becker, M. Braack, and R. Rannacher. Numerical simulation of laminar flames at low Mach number by adaptive finite elements. *Combust. Theory Modelling*, 3:503–534, 1999.

BE01

BE01. E. Burman and A. Ern. Nonlinear crosswind diffusion and discrete maximum principle for stabilised Galerkin approximations. Technical Report 2001–204, CERMICS-ENPC, Marne la Vallée, France, 2001. http://cermics.enpc.fr/reports/CERMICS-2001-204.ps.gz.

BH82

BH82. A.N. Brooks and T.J.R. Hughes. Streamline Upwind/Petrov–Galerkin formulations for convective dominated flows with particular emphasis on the incompressible Navier–Stokes equations. *Comput. Methods Appl. Mech. Engrg.*, 32:199–259, 1982.

BR96

BR96. R. Becker and R. Rannacher. A feed-back approach to error control in finite element methods: basic analysis and examples. *East-West J. Numer. Math.*, 4(4):237–264, 1996.

BR01

BR01. R. Becker and R. Rannacher. An optimal control approach to a posteriori error estimation in finite element methods. *Acta Numerica*, 2001. to appear.

Br98

Bra98. M. Braack. *An Adaptive Finite Element Method for Reactive Flow Problems*. PhD thesis, Heidelberg University, 1998.

BS2

BS98. B.A.V. Bennett and M.D. Smooke. Local rectangular refinement with application to axisymmetric laminar flames. *Combust. Theory Modelling*, 2(3):221–258, 1998.

BS1

BS99. B.A.V. Bennett and M.D. Smooke. Local rectangular refinement with application to nonreacting and reacting fluid flow problems. *J. Comput. Physics*, 151:684–727, 1999.

Ch94

Che94. K. Chen. Error equidistribution and mesh adaption. *SIAM J. Sci. Comput.*, 15(4):798–818, 1994.

CKM83

CKM83. T.P. Coffee, A.J. Kotlar, and M.S. Miller. The overall reaction concept in premixed, laminar, steady-state flames. I. Stoichiometries. *Combust. Flame*, 54:155–169, 1983.

CP93

CP93. P.J. Coelho and J.C.F. Pereira. Calculation of a confined axisymmetric laminar diffusion flame using a local grid refinement technique. *Combust. Sci. Technol.*, 92:243–264, 1993.

CV99

CV99. C. Carstensen and R. Verfürth. Edge residuals dominate a posteriori error estimators for low-order finite element methods. *SIAM J. Numer. Anal.*, 36:1571–1587, 1999.

DB00

DB00. M.S. Day and J.B. Bell. Numerical simulation of laminar reacting flows with complex chemistry. *Combust. Theory Modelling*, 4:535–556, 2000.

LG94

dd94. H.C. de Lange and L.P.H. de Goey. Numerical modelling in a locally refined grid. *Int. J. Num. Mech. Eng.*, 37:497–515, 1994.

EG94

EG94. A. Ern and V. Giovangigli. *Multicomponent Transport Algorithms*, volume m24 of *Lecture Notes in Physics*. Springer, Heidelberg, 1994.

EG98

EG98. A. Ern and V. Giovangigli. Thermal diffusion effects in hydrogen-air and methane-air flames. *Combust. Theory Modelling*, 2:349–372, 1998.

FF92

FF92. L.P. Franca and S.L. Frey. Stabilized finite element methods: II. The incompressible Navier–Stokes equations. *Comput. Methods Appl. Mech. Engrg.*, 99:209–233, 1992.

Gi99

Gio99. V. Giovangigli. *Multicomponent Flow Modelling.* Modelling and Simulation in Science, Engineering and Technology. Birkhäuser, Boston, 1999.

GS89

GS89. V. Giovangigli and M.D. Smooke. Adaptive continuation algorithms with application to combustion problems. *Appl. Numer. Math.*, 5:305–331, 1989.

JNP84

JNP84. C. Johnson, U. Nävert, and J. Pitkäranta. Finite element methods for linear hyperbolic equations. *Comput. Methods Appl. Mech. Engrg.*, 45:285–312, 1984.

Jo87

Joh87. C. Johnson. *Numerical Solution of Partial Differential Equations by the Finite Element Method.* Cambridge University Press, Cambridge, 1987.

JSW87

JSW87. C. Johnson, A. Schatz, and L. Wahlbin. Crosswind smear and pointwise error in streamline diffusion finite element methods. *Math. Comp.*, 49:25–38, 1987.

KN80

KN80. J. Kautsky and K. Nichols. Equidistributing meshes with constraints. *SIAM J. Sci. Stat. Comput.*, 1(4):499–511, 1980.

Lu92

Lub92. G. Lube. An asymptotically fitted finite element method for convection dominated convection-diffusion-reaction problems. *Math. Mech.*, 72:189–200, 1992.

MLVG95

Mdvd95. R.M.M. Mallens, H.C. de Lange, C.H.J. van de Ven, and L.P.H. de Goey. Modeling of confined and unconfined laminar premixed flames on slit and tube burners. *Combust. Sci. Technol.*, 107:387–401, 1995.

MS85

MS85. A. Majda and J. Sethian. The derivation and numerical solution of the equations for zero Mach number combustion. *Combust. Sci. Technol.*, 42:185–205, 1985.

Pax99

Pax99. S. Paxion. *Développement d'un solveur multigrille non-structuré parallèle pour la simulation de flammes laminaires en chimie et transport complexes.* PhD thesis, EM2C, ECP, Paris, 1999. PhD dissertation.

Pal98

PHB+98. R.B. Pember, L.H. Howell, J.B. Bell, P. Colella, W.Y. Crutchfield, W.A. Fiveland, and J.P. Jessee. An adaptive projection method for unsteady, low-Mach number combustion. *Combust. Sci. Technol.*, 140:123–168, 1998.

Re93

Reb93. S. Rebay. Efficient unstructured mesh generation by means of Delaunay triangulation and Bowyer-Watson algorithm. *J. Comput. Phys.*, 106:125–138, 1993.

SG95

Sd95. L.T. Somers and L.P.H. de Goey. A numerical study of a premixed flame on a slit burner. *Combust. Sci. Technol.*, 108:121–132, 1995.

SE99

SE99. Y.T. Shih and H.C. Elman. Modified streamline diffusion schemes for convection-diffusion problems. *Comput. Methods Appl. Mech. Engrg.*, 174:137–151, 1999.

TV96

TV96. L. Tobiska and R. Verfürth. Analysis of a streamline diffusion finite element method for the Stokes and Navier–Stokes equations. *SIAM J. Numer. Anal.*, 33(1):107–127, 1996.

Wi85

Wil85. F.A. Williams. *Combustion Theory.* Addison-Welsey, second edition, 1985.